Sea Surface Wind Direction Retrieval Based on Convolution Neural Network and Wavelet Analysis

Chaogang Guo , Weihua Ai, Shensen Hu, Xiaoyong Du, and Nan Chen

Abstract—Sea surface wind streak is one of many geophysical phenomena in synthetic aperture radar (SAR) images, which is often used to obtain sea surface wind direction. At present, the recognition of wind streaks mainly depends on artificial experience, and the recognition efficiency and accuracy are not high. In this article, the transfer learning based convolutional neural network architecture of Inception v3 was introduced to the recognition of sea surface wind streaks. Four categories of geophysical phenomena imaged by Gaofen-3 (GF-3) SAR from 2019 to 2020 were chosen for retraining of the full pre-retrained Inception v3 model. Then, we use the retrained model to identify the wind streak of GF-3 in 2018 and use it to retrieve the sea surface wind direction. The results show that the transfer learning method is effective. The recognition accuracy of the model can reach 92.0% and 95.2% after data is augmented. Compared with the reanalysis data of European Centre for Medium-Range Weather Forecasts, the root-mean-square error of the retrieved wind direction is 9.12°, which further verifies the ability of the training model to identify wind streaks.

Index Terms—Gaofen-3 (GF-3), Inception v3 model, sea surface wind direction, synthetic aperture radar (SAR), wind streak (WS).

I. Introduction

SEA surface wind field is an important parameter in the interaction between atmosphere and ocean, which has an important impact on maritime shipping, marine environment, maritime search, rescue, etc. At present, satellite loads commonly used to detect sea surface wind field include scatterometer [1], radiometer [2], altimeter [3], and synthetic aperture radar (SAR) [4]. SAR is a microwave remote sensing radar with the capability of all-day, all-weather and high-resolution imaging. It can observe the earth on the scales of 0.5–5 km, which is almost impossible for other sensors [5]. However, SAR has only one antenna and is unable to retrieve wind direction and wind speed at the same time through rotating antenna or observation of multiple antennas like scatterometer. Therefore, it is necessary to obtain the sea surface wind direction before SAR uses a geophysical model function to retrieve the sea surface wind speed. There are usually two methods to obtain the wind direction for retrieval. One is to use the external wind direction, such as the wind direction of a numerical weather prediction model. The other is to extract the wind direction from the linear streak of the SAR image [6].

Due to the instability of the ocean-atmospheric boundary layer, there are periodic streaks parallel to the sea surface wind direction on SAR images, which are called wind streaks (WSs) [7]. The sea surface wind direction can be inferred from the WSs on the SAR image. However, WSs do not appear in all SAR images and can be clearly observed, which is also the biggest defect of wind direction retrieval based on WSs. In fact, WSs generally appear in the sea area with slightly higher wind speed and unstable atmospheric conditions [8]. Statistics showed that about 92.6% of the WS occur when the wind speed is greater than 6 m/s, and about 67.3% of the WS occur under unstable atmospheric conditions [9]. Levy [9], [10] counted about 2000 images of RADARSAT Scan-SAR. The results showed that only about 44% of SAR images can use WSs to retrieve sea surface wind direction, and the distribution of WSs has obvious seasonality and regionality. The probability distribution of WSs is uneven in global waters. Zhao *et al.* [8] found that about 48% of the SAR images contain obvious WSs based on 227 Terra SAR-X and Tan DEM-X images of the European North Sea and Baltic Sea. Yi *et al.* [11] found no obvious linear texture more than 50% of the SAR images. In addition, Chang *et al.* [12] proposed that not every image contains WS features, and there may be other linear features similar to WSs caused by atmospheric and ocean internal waves in the SAR image. To effectively use the WS information in SAR images, it is necessary to quickly recognize the data containing WS features from a large number and a wide variety of SAR images. At present, the identification of WSs mainly depends on manual experience. The recognition speed is slow and the efficiency is low, which is far from meeting the needs.

In recent years, deep learning has shown great potential and is widely used in speech recognition, image recognition, and other fields. The convolutional neural network (CNN) is one of the representative algorithms of deep learning. Compared with a neural network, a CNN greatly reduces the number of model parameters and improves the training efficiency [13]. CNN was originally proposed by LeCun. The model network can extract image features such as color, texture, and shape by itself, and has obvious advantages in image processing [14]. Chen *et al.* [15] classified the geophysical phenomena contained in the WV model data of Sentinel-1 satellite by using the Inception v3 model based on CNN. The overall accuracy of the ten categories of geophysical phenomena exceeded 93%. This model realizes the classification of 20 × 20 km scale geophysical phenomenon
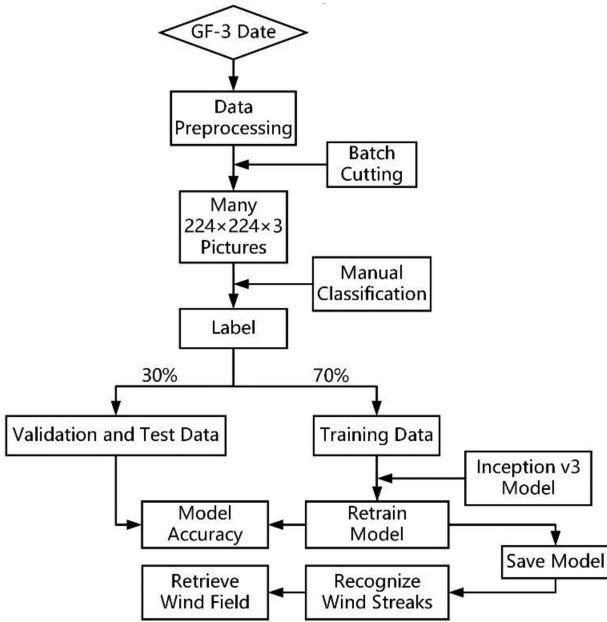
Fig. 1.   Flowchart of model retraining and wind direction retrieval.

collected by Sentinel-1 WV model. However, Gaofen-3 (GF-3) QPS mode SAR image can realize sea surface wind field retrieval with 3 × 3 km resolution based on WSs [16], [17], which puts forward higher requirements for the scale of geophysical phenomenon recognition.

To realize smaller-scale WS recognition, we tried to fine-tune the Inception v3 model pretrained in ImageNet Database, and retrained the model by using the WSs identified in GF-3 SAR and the phenomena similar to WSs. The rest of this article is organized as follows: Section II describes the GF-3 SAR data and Inception v3 model architecture used, data preprocessing process, data augment method, and wind direction retrieval method in this study. In Section III, we evaluate the performance of the model based on transfer learning, and compare the retrieved wind direction of the WS recognized by the retraining model with the European Centre for Medium-Range Weather Forecasts (ECMWF) reanalysis data. Discussion and perspectives are made in Section IV. The whole process of model retraining and wind direction retrieval is shown in Fig. 1.

II. DATA AND METHOD

A. GF-3 QPSI Data

GF-3 launched by China in October 2016 is a high-resolution, fully polarized SAR satellite. Its SAR sensor has 12 imaging modes, which is the sensor with the most imaging modes in the world. The SAR payload has to support operation in single-polarization (HH or VV), dual-polarization (HH+HV or VH+VV), and quad-polarization (HH+HV+VH+VV) with respect to the observing modes [18]. In this study, QPSI model VV polarization data commonly used to retrieve wind fields are used. The width of one pixel of the mode data is about 2.25 m and the height is about 5.13 m. An image usually covers an area of 25–35 km.

Establishing an appropriate data set of geophysical phenomena can help to analyze the relationship between phenomena and physical processes. Wang *et al.* [19] systematically summarized the theory of geophysical phenomena contained in spaceborne SAR images, defined 10 geophysical phenomena for WV mode SAR images of Sentinel-1 in Europe, and established data sets using more than 37 000 SAR subimages.

At present, GF-3 has not released the official sea surface geophysical phenomena data set. We label the collected data according to the characteristics and texture structure of the geophysical phenomenon. In addition to WSs, we also identified three categories of geophysical phenomena with similar characteristics to WSs: biological slicks (BSs), pure ocean waves (POWs), and microconvective cells (MCCs). The generation conditions of four categories of geophysical phenomena and their performance characteristics in SAR images are as follows: WS is a rolling sea surface imprint of the atmospheric boundary layer, which usually occurs in neutral atmosphere or unstable stratification. It is shown as periodic and quasi two-dimensional (2-D) roll patterns like black-and-white streaks with wavelengths ranging from 0.8 to 5 km in SAR images, and some small patterns of WSs contain cell shaped patterns. BSs in the ocean are natural films that accumulate at the water–air boundary, which is usually visible as dark filaments on SAR images. POWs are characterized by continuous periodic waves with wavelengths ranging from 0.1 to 0.8 km, and often coexist with other atmospheric and marine phenomena. MCC is a cellular updraft or downdraft generated by strong vertical convective movement due to the temperature difference between the atmosphere and the ocean. It shows coherent periodic cell shape and roll pattern similar to that in the WS on the SAR image [19]–[22].

We collected 1435 scenes GF-3 SAR data from July 2018 to July 2020 in QPSI mode. There are 1257 scenes geophysical phenomenon in the above four categories, and the data of 178 scenes geophysical phenomenon that do not belong to the above are labeled as other geophysical phenomena. It is worth noting that in addition to these geophysical phenomena used in this study, SAR can also monitor other geophysical phenomena, such as atmospheric front, sea ice (SI), and oceanic front. The quantity distribution of various phenomena is shown in Fig. 2. The data of 2019 and 2020 are used to retrain the pretrained Inception v3, and then use the retrained model to identify the geophysical phenomena in 2018.

WSs usually appear as black-and-white streaks in SAR images [23], but other geophysical phenomena also contain similar structures. In addition to BS, POW, and MCC used in this study, the effects of coastline, atmospheric internal wave, ocean internal wave and SI edge will also lead to texture information similar to WSs in SAR images [24], but these collections are so small that they are not added to dataset. Therefore, it is a challenging task to accurately recognize WSs from various geophysical phenomena.

B. Inception V3 Model and Transfer Learning

Inception Net is one of the CNN models, which was first used by Google in the ImageNet large scale visual recognition
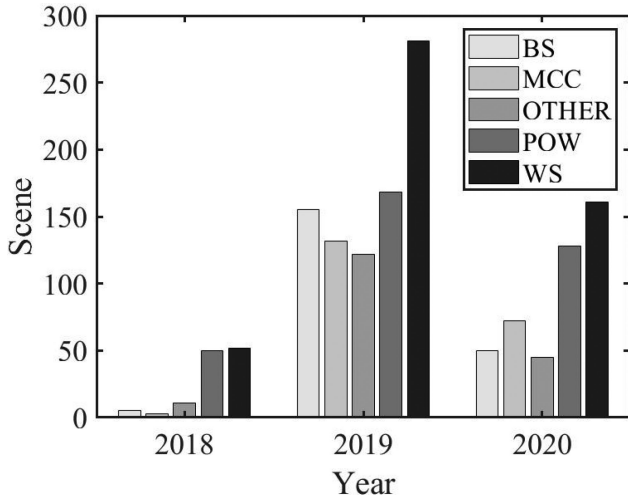
Fig. 2. Quantity distribution of various geophysical phenomena collected from 2018 to 2020.
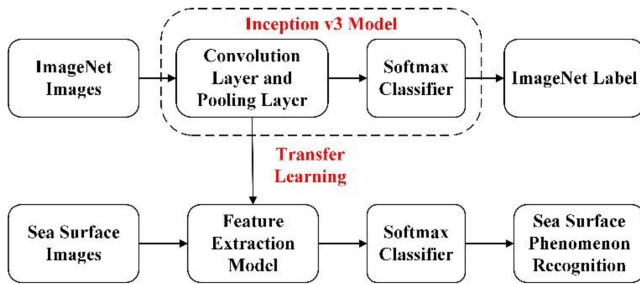

Fig. 3. Transfer learning architecture based on Inception v3 model.

challenge of ImageNet in 2014 [25]. Inception net has four versions, i.e., v1 to v4. Inception v3 model was used in this study, which divides a larger 2-D convolution kernel into two smaller 1-D convolution kernels in the Inception v2 model, and optimizes the architecture of the Inception module. The model effectively reduces the number of model parameters, further improves the ability of the model to suppress overfitting, and reduces the top-5 error rate from 4.8% to 3.5%. Inception v3 model has been able to extract general features such as curves and edges used in SAR images [26]. Benefiting from the architecture of Inception v3, the model is widely used in transfer learning.

Inception v3 is a very deep network with 48-layer network architecture and more than 23 million trainable parameters. Therefore, training a new Inception v3 model requires a large number of data sets, a long time and high hardware conditions. But we can achieve the classification function through transfer learning and avoid this process. The research shows that by retaining the settings of all convolution layers and changing the structure of the full connection layer, an Inception v3 model can well realize the recognition and classification of new images. As shown in Fig. 3, the Inception v3 model is usually composed of two main parts: 1) convolution layer and pooling layer to extract image features and 2) Softax and full connection layer

are used for image classification [27]. We tried to use the image feature extraction part of the pre-trained Inception v3 model to extract the features of geophysical phenomena directly. By training our reconstructed softmax layer and completing the connection layer, we could realize the recognition of geophysical phenomena. The advantage of transfer training is that Inception v3 architecture with most parameters reserved has the ability to recognize image edges and textures. Only a small amount of data is needed to train the newly added architecture so that the new model can have the ability to recognize geophysical phenomena.

C. Data Preprocessing and Making Data Sets

GF-3 ground system produces level 1 (L1) and level 2 (L2) standard products. L1A product is a single look complex product, L1B product includes a single look product and a multilook product, and L2 product is a system geometric correction product. In this study, L1A product is used, which retains amplitude, phase, and polarization information and can provide oblique ground conversion coefficient.

The resolution of L1A is inconsistent in azimuth and range, and there are problems such as speckle noise. Before using the data, it is necessary to carry out image preprocessing such as radiometric calibration, multilook processing, geometric correction, etc. The first is to calibrate the original data. In fact, calibration is to establish the relationship between radar image and detection area backscattering coefficient. This process is to convert the dimensionless brightness value recorded by SAR into radar backscattering coefficient. According to the user manual, the L1A data calibration formula is as follows:

$$\sigma_{dB}^0 = 10\log_{10}\left(P^I * \left(\frac{\text{Qualify Value}}{32767}\right)^2\right) - K_{dB} \quad (1)$$

where $P^I = I^2 + Q^2$, P^I is SAR complex image power, I is the amplitude of the real part of the image, Q is the amplitude of the imaginary part of the image, Qualify Value is the maximum value before image quantization, and K_{dB} is the calibration constant.

The azimuth resolution of SAR image is usually higher than the range resolution, and the formation mechanism of the two is not related, resulting in the inconsistency of the ground range resolution. On the one hand, multilook processing can reduce the speckle noise of the image, on the other hand, it can make the resolution of azimuth and range to be consistent and improve the image quality.

In this experiment, combined with the demand of 224 × 224 pixels in the CNN model dataset image, the ground distance resolution and azimuth resolution obtained by multilook processing are close to 11 m, so the size of each subimage is about 2.5 km.

Due to the earth rotation, satellite flying attitude and the side looking mechanism of SAR radar, the detected SAR image will be geometrically deformed relative to the actual geographical position. To ensure the accuracy of spatial information of data, the image will be geometrically corrected after radiometric correction to eliminate the distortion in the original data.
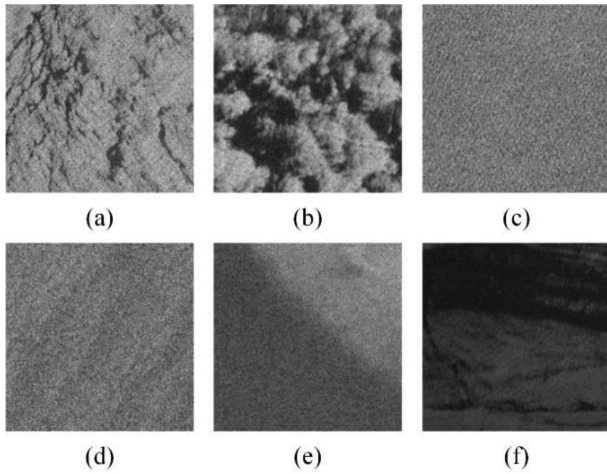
Fig. 4. Example of geophysical phenomena. (a) BSs. (b) MCC. (c) POWs. (d) WSs. (e) and (f) Other geophysical phenomena (OTHER).
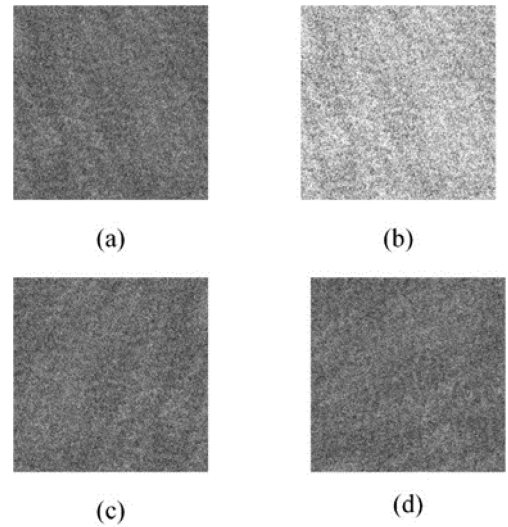

Fig. 5. Data augmentation method. (a) Original data subimage. (b) Image after brightness change. (c) Image after flipping. (d) Image after rotation.

After preprocessing, the image size of GF-3 SAR is usually large. On the one hand, such an image is not compatible with Inception v3. On the other hand, a too-large image may contain a variety of geophysical phenomena at the same time, which affects the accuracy of model training. Therefore, each scene image is cropped into several 224×224 pixels subimages. To ensure the balance of various geophysical phenomena, we screened 1000 images for each kind of phenomena from the cropped subimages, and established a data set with a data volume of 5000, called the original data set (ODA). In the above phenomenon screening, we mainly based on two standards: one is that there is only one geophysical phenomenon in the subimage, and the other is that a geophysical phenomenon is dominant in the subimage. Examples of the geophysical phenomenon are shown in Fig. 4.

Although transfer learning does not need a very large data set, to improve the generalization ability of the model and avoid overfitting in the training process, this article uses augmentation to expand the data set. By flipping, randomly rotating and changing the brightness, the data set was expanded to 4000 images of each kind of geophysical phenomenon, and another data set containing 20000 SAR images is established, which is called augmented data set (ADA). Example images by data augmented are shown in Fig. 5.

D. Wind Direction Retrieval Method

The methods of retrieving sea surface wind direction based on WS of SAR image include local gradient (LG), 2-D fast Fourier transform (FFT) and wavelet analysis. The wind direction retrieved by these methods has 180 ° ambiguity, which needs to be eliminated with the help of other data [28], [29]. 2-D FFT calculates the spectral distribution of the image. The wind direction is orthogonal to the direction of the main spectral energy, and the standard deviation of the wind direction is 10°–37°. It is usually used for large-scale retrieval, such as 20×20 km. LG uses the standard image processing algorithm to calculate the LG. The wind direction is orthogonal to the most frequent
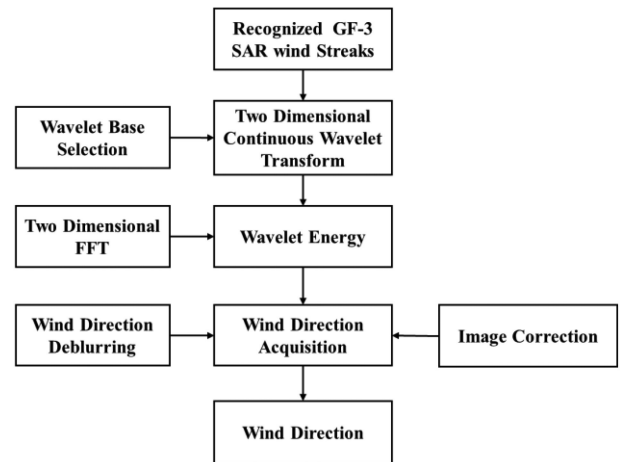

Fig. 6. Flowchart of SAR sea surface wind direction retrieval based on wavelet analysis and Inception v3 model.

gradient direction. The error of the wind direction relative to the buoy is about 20°, and the minimum spatial sampling is 10 km $\times$ 10 km. Wavelet analysis can realize the localization function in time domain and frequency domain at the same time, and can automatically adjust the time-frequency window to meet the actual analysis needs. The error accuracy of wind direction retrieval can be better than LG and 2-D FFT by selecting the appropriate wavelet basis for 2-D continuous wavelet transform (CWT) of SAR image. The specific retrieval process is shown in Fig. 6. The wavelet basis function can be expressed as

$$\Psi_{a,b}(t) = |a|^{-1/2} \Psi\left(\frac{t-b}{a}\right) \quad a, b \in R, a \neq 0 \quad (2)$$

where $\Psi_{a,b}(t)$ is the result of translation and scaling by wavelet generating function $\Psi(t)$. a is called the scaling factor and b is called the scaling factor. The process of decomposing any signal by using this set of wavelet basis functions is called

wavelet transform, which projects the function to the whole function family. The 2-D Mexican-hat wavelet transform used in this study has achieved good retrieval results in previous experiments [30]. 2-D Mexican-hat can be expressed as

$$\Psi\,(x,y) = \left(2 - \left(x^2 + y^2\right)\exp\left(-\frac{x^2 + y^2}{2}\right)\right). \quad (3)$$

SAR image can be regarded as a 2-D signal and needs 2-D CWT, which can be expressed as

$$(W_\Psi f)\,(a_x,b_x;a_y,b_y) = \int_{-\infty}^{+\infty}\int_{-\infty}^{+\infty} \bar{\Psi}_{(a_x,b_x)}\,(x)$$
$$\times \bar{\Psi}_{(a_y,b_y)}\,(y)\ f\,(x,y)\,dxdy \quad (4)$$

where $(W_\Psi f)(a_x,b_x;a_y,b_y)$ is the wavelet coefficient obtained after 2-D CWT. For the 2-D image signal, the wavelet transform obeys the law of energy conservation, and the energy conservation formula of the 2-D signal can be expressed as

$$E_f = \int_{-\infty}^{+\infty}\int_{-\infty}^{+\infty} |f\,(x,y)|^2 dxdy = \int_{-\infty}^{+\infty}\frac{E_w\,(a)}{C_\Psi a^2}da \quad (5)$$

where $C_\Psi = \int_{-\infty}^{+\infty}(|\Psi(w)|^2/|w|)dw$ is a permissive condition. $E_w\,(a) = \int_{-\infty}^{+\infty}|(W_\Psi f)_a\,(x,y)|^2 dxdy$ is the wavelet energy spectrum related to the scale factor a of 2-D continuous wavelet. The wavelet energy spectrum images at different scales are analyzed to obtain the WS information of SAR image.

Then, 2-D FFT is performed on the energy spectrum graph to calculate the spectral number of WS in SAR image. The 2-D FFT can be expressed as

$$Y_{l,m} = \sum_{j=1}^{N}\sum_{k=1}^{N} X_{j,k}\exp\left(\frac{-2\pi\,(jl + km)}{N}\right) \quad (6)$$

where $Y_{l,m}$ is the spectral number of WSs in SAR image, and X is the image gray value, $m = 1,2,\ldots,N$, and $l = 1,2,\ldots,N$. Finally, the line connecting the 2-D wave number spectrum peak is made a vertical line, and the sea surface wind direction is obtained after deblurring the wind direction. Aiming at the problem of 180° ambiguity in the retrieval of wind direction by Mexican-hat wavelet method, ECMWF is used to analyze the wind direction of the wind field and remove it.

Combined with the retrained model, the flow of SAR WS recognition and wind direction retrieval is shown in Fig. 7. First, the SAR image of a scene 2018 is preprocessed, and then the scene data is cut into several 224 × 224 pixels subimages from top to bottom and left to right, and numbered in order. These subimages are recognized using the retrained Inception v3 model. The subimage recognized by the model as WS is input into the 2-D Mexican-hat wavelet transform model to retrieve the wind direction, otherwise the wind direction of the subimage is represented by ECMWF reanalysis data. Finally, the wind directions of all subimages are combined according to the previous numbers to obtain the wind direction information of an SAR image.
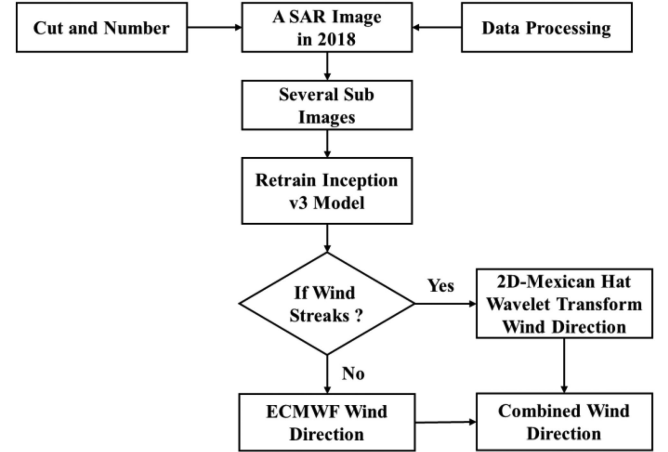

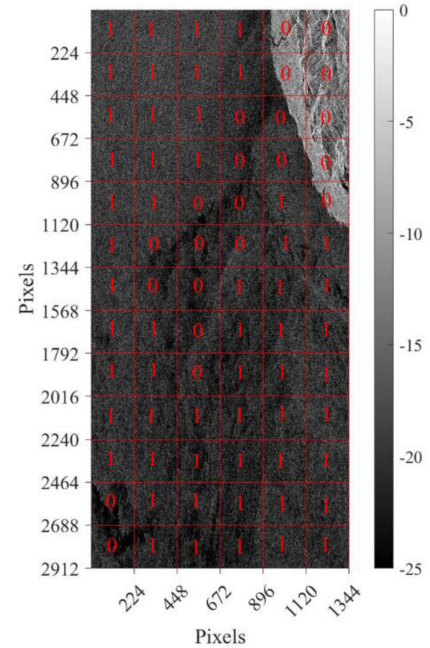Fig. 7. Flowchart of wind retrieval from GF-3 2018 SAR image.

Fig. 8. As a result of subimage recognition of one scene SAR data, "1" represents the WS region and "0" represents the nonWS region.

In SAR images, some subimages may have WS features, whereas the rest are other geophysical phenomena. Therefore, in a scene SAR image, the subimages identified as WSs are marked as "1" and the rest are marked as "0," as shown in Fig. 8. More than 90% of the subimages in scene SAR data are identified as WSs, and the image is defined as WSs data. The wind direction retrieved from these WS data is compared with ECMWF reanalysis data.

III. EXPERIMENTAL RESULT

A. Retrain Process and Preliminary Analysis

The two data sets (ODA and ADA) were randomly divided into three parts: training set, validation set and test set.
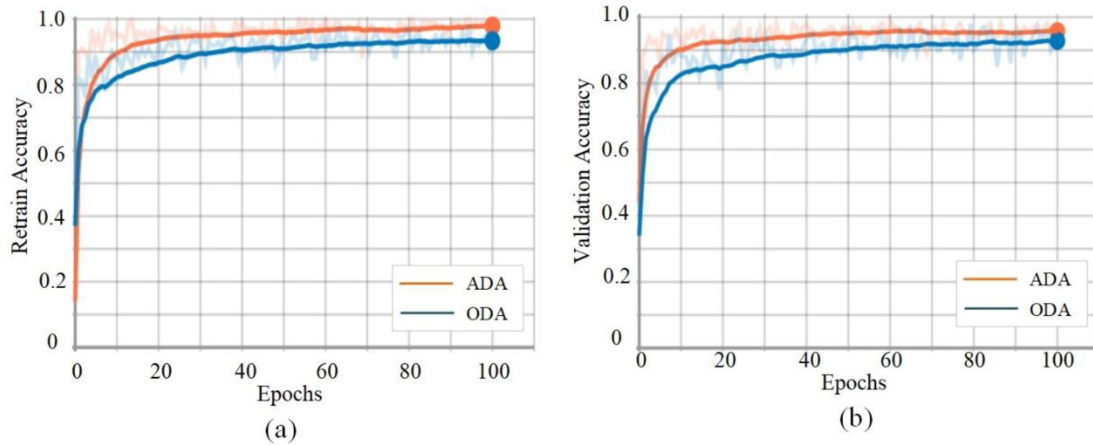
Fig. 9.   Accuracy of training set and test set of ODA and ADA. (a) Retrain accuracy. (b) Validation accuracy.

TABLE I
PERFORMANCE OF ODA SET AND ADA SET

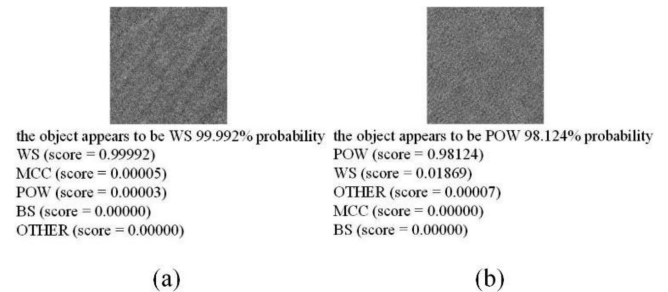| Data Set	Category	Performance
Original data set	Training set accuracy	92%–94%
	Validation set accuracy	91%–92%
	Test set accuracy	92.0%
Augmented data set	Training set accuracy	96%–98%
	Validation set accuracy	94%–96%
	Test set accuracy	95.2%

Fig. 10.   Recognition results of 2018 GF-3 SAR subimages using a retrain model.

The proportion of each part was 7:2:1. Fig. 9 shows the accuracy of retrain and validation based on transfer learning model, Fig. 9(a) is the curve of retrain accuracy with epoch and Fig. 9(b) is the validation accuracy with epochs. As shown, at first, the accuracy of both data sets increases rapidly with the epochs, and after about 20 epochs, the change of accuracy tended to be stable. The accuracy of training set and validation set of ADA are higher than that of ODA.

According to the changes in accuracy, we summarized the results and get Table I. The test set accuracy of the ODA can reach 92%, and that of the ADA set can reach 95.2%. According to the change of accuracy, it is preliminarily determined that the Inception v3 model based on transfer learning can recognize 4 geophysical phenomena. Data augmented can improve the accuracy of model recognition. We selected the model trained by ADA as the model for the follow-up experiment, which is called ADA model.

To further verify the ability of the model to recognize sea surface WSs. After completing the retraining of fine-tuning model, we use the ADA model to identify the GF-3 data in 2018. An example of the recognition result of WSs and POW of a phenomenon is shown in Fig. 10. For each recognition result, the first line gives the result of model classification, and the second to sixth lines give the probability that the model recognizes the image as various phenomena.

B. Retrieval Wind Direction Results

ADA model identified 150 scenes of GF-3 SAR WS data from 2018 to 2020 for wind direction retrieval. The average value of sea surface wind direction obtained by retrieval of each scene data is compared with ECMWF reanalysis wind field data. First, the process of retrieving sea surface wind direction from GF-3 SAR data is explained by using the data that all subimages of a single scene are WSs. The scene data are located in the northern Indian Ocean. The imaging time is 01:42 (UTC) on July 8, 2018. The central longitude and latitude are 62.9° E and 21.7° N, covering an area of about 24×13 km. The time of reanalysis data of ECMWF for comparison is 02:00 (UTC) on July 8, 2018, about 18 min away from GF-3 data, and the coordinates are 63.0° E and 21.75° N, as shown by the red dot in Fig. 11(a).

We use the 2-D Mexican-hat retrieval of 2.5 km resolution wind direction. The white short line in Fig. 11(a) is the wind direction obtained by 2-D Mexican-hat retrieval. The actual wind direction is possible at both ends of the short line. According to the fact that the ECMWF wind direction is southwest wind at this time, as shown by the red arrow in Fig. 11(b), the final retrieval wind direction result can be determined, as shown by the white arrow in Fig. 11(b). It can be seen from the texture characteristic in the image that the linear characteristic of the WS is close to the retrieved wind direction. The average of the retrieved
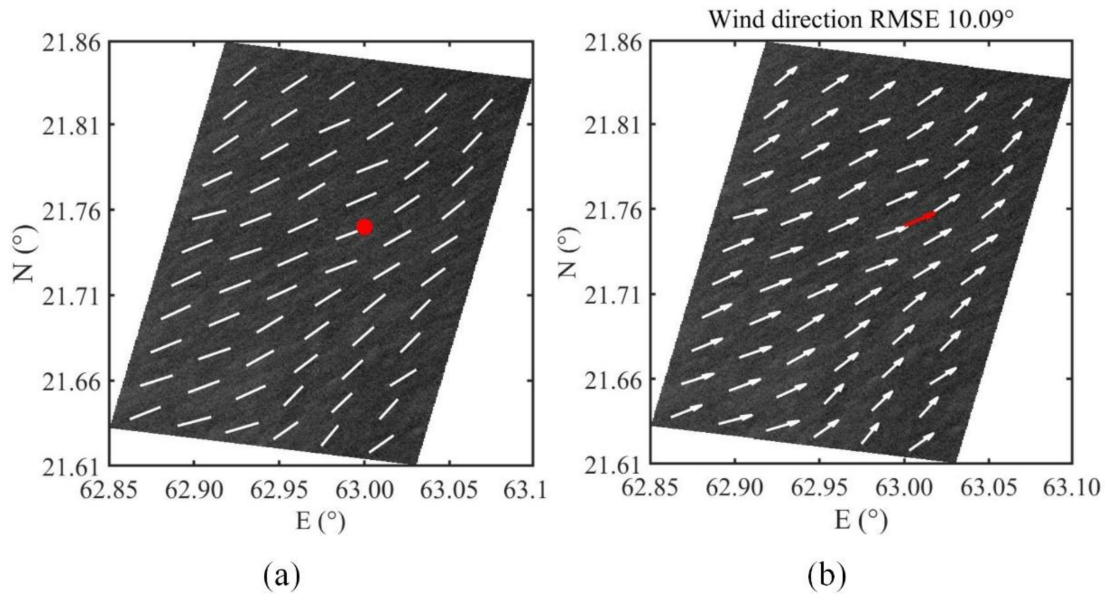
Fig. 11. Retrieval results of GF-3 image obtained at 01:42 (UTC) on July 8, 2018. (a) Wind direction with 180° ambiguity retrieval by 2-D Mexican-hat. (b) Real wind direction deblurring by ECMWF reanalysis data.
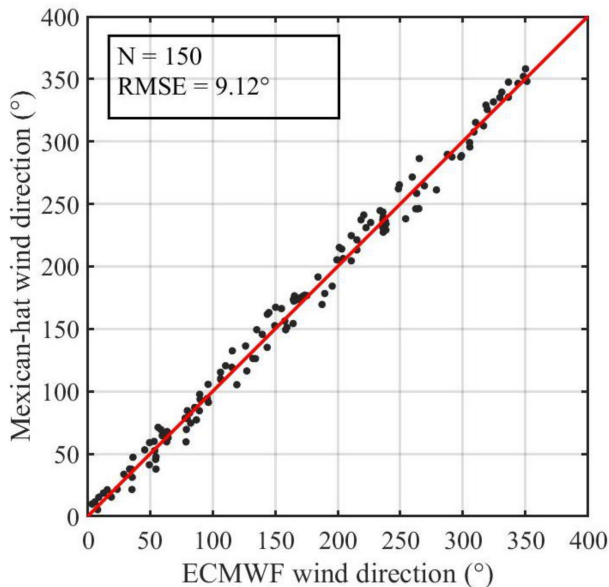

Fig. 12. Wind direction retrieved from 150 scenes GF-3 SAR data and wind direction reanalyzed by ECMWF.

wind direction by 2-D Mexican-hat is 227.50°, the sea surface wind direction provided by the reanalysis data of ECMWF is 236.41°, which is 9.91° different from the retrieval result, and the root-mean-square error of the retrieved wind direction is 10.09°.

Referring to the above method, the wind direction retrieval results of 150 scenes WS data are shown in Fig. 12. It can be seen from the figure that the average sea surface wind direction retrieved from most data is close to the ECMWF reanalysis wind field data, and the root mean square error of wind direction retrieved from 150 scenes data is 9.12°.

IV. DISCUSSION AND PERSPECTIVES

With the continuous progress of spaceborne ocean exploration technology, it is very necessary to realize rapid and automatic identification of WSs on the sea surface from many geophysical phenomena. In this article, the concept V3 model based on CNN is used to identify sea surface WSs. Through the methods of data preprocessing and data enhancement, the VV polarization data of GF-3 SAR QPSI mode from 2019 to 2020 are constructed into the data set to retrain. By retraining the model, SAR sea surface WS recognition based on transfer learning is realized.

The recognition and classification of geophysical phenomena observed in SAR images play an important role in studying the microphysical process of atmospheric ocean interaction and the regional and seasonal distribution of geophysical phenomena. For example, with the melting of Arctic SI, more and more ships will try to use Arctic waterways as navigation routes in special seasons. Although people usually sail in the warmer Arctic season and are equipped with professional icebreakers, different SI densities and thicknesses will still pose varying degrees of threats to ship navigation. However, SI can be identified according to the observation images of spaceborne SAR images, and appropriate routes can be planned according to the distribution of SI, which can effectively reduce navigation costs and possible dangers [31]. At present, spaceborne SAR technology is becoming more and more perfect. A single SAR satellite can also collect a large number of sea surface images, but there is little research on automatic recognition and classification based on geophysical phenomenon types. Taking the WSs that can obtain the sea surface wind direction as an example, the Inception v3 model based on transfer learning is used to identify and verify the performance of WSs and three phenomena with similar structural characteristics. This work provides a method

for quickly identifying SAR images with WS features, and makes a new attempt to broaden the application of SAR data.

The Inception v3 model based on transfer learning preliminary has the ability to recognize sea surface WSs. However, it cannot be ignored that there are still many challenges. On the one hand, this experiment only uses geophysical phenomena similar to the WS structure, and the actual SAR can also monitor many geophysical phenomena. On the other hand, our model values are for the case where there is only one geophysical phenomenon in the image, but sometimes there are many geophysical phenomena in one scene image. In addition, GPM can provide 3-D rainfall parameters and can also be used to measure sea surface wind field. On this basis, the physical process of rain–wind–wave interaction can be further studied [32], [33]. This is our future research work.

REFERENCES

[1] D. G. Long and J. M. Mendel, "Identifiability in wind estimation from scatterometer measurements," *IEEE Trans. Geosci. Remote Sens.*, vol. 29, no. 2, pp. 268–276, Mar. 1991.

[2] S. H. Yueh, W. J. Wilson, S. J. Dinardo, and S. V. Hsiao, "Polarimetric microwave wind radiometer model function and retrieval testing for WindSat," *IEEE Trans. Geosci. Remote Sens.*, vol. 44, no. 3, pp. 584–596, Mar. 2006.

[3] R. E. Glazman and A. Greysukh, "Satellite altimeter measurements of surface wind," *J. Geophys. Res., Oceans*, vol. 98, no. C2, 1993, Art. no. 2475.

[4] J. Horstmann, H. Schiller, J. Schulz-Stellenfleth, and S. Lehner, "Global wind speed retrieval from SAR," *IEEE Trans. Geosci. Remote Sens.*, vol. 41, no. 10, pp. 2277–2286, Oct. 2003.

[5] K. B. Katsaros, P. W. Vachon, W. T. Liu, and P. G. Black, "Microwave remote sensing of tropical cyclones from space," *J. Oceanogr.*, vol. 58, no. 1, pp. 137–151, 2002.

[6] F. M. Monaldo, D. R. Thompson, W. G. Pichel, and P. Clemente-Colón, "A systematic comparison of QuikSCAT and SAR ocean surface wind speeds," *IEEE Trans. Geosci. Remote Sens.*, vol. 42, no. 2, pp. 283–291, Feb. 2004.

[7] W. Alpers and B. Brümmer, "Atmospheric boundary layer rolls observed by the synthetic aperture radar aboard the ERS-1 satellite," *J. Geophys. Res. Oceans*, vol. 99, no. C6, pp. 12613–12621, 1994.

[8] Y. Zhao, *Research on Ocean Wind Field Detection by Spaceborne Synthetic Aperture Radar*. Beijing, China: Univ. Chin. Acad. Sci. (Inst. Remote Sens. Digit. Earth, Chin. Acad. Sci.), 2017.

[9] G. Levy, "Imaging boundary layer roll signatures for climate applications," in *Proc. IEEE Int. Geosci. Remote Sens. Symp.*, 1998, vol. 3, pp. 1437–1438.

[10] G. Levy, "Boundary layer roll statistics from SAR," *Geophys. Res. Lett.*, vol. 28, no. 10, pp. 1993–1995, 2001.

[11] Z. Yi, J. Xinwei, and S. Qingchao, "Ocean wind retrieval from synthetic aperture radar images based on external initial wind direction," *Remote Sens. Technol. Appl.*, vol. 26, no. 4, 2011, Art. no. 694.

[12] J. Chang, *Research on Offshore Wind Energy Resources Remote Sensing Technology and Applications Based on the Satellite-Borne SAR*. Qingdao, China: Ocean Univ. China, 2012.

[13] S. Indolia, A. K. Goswami, S. P. Mishra, and P. Asopa, "Conceptual understanding of convolutional neural network—A deep learning approach," *Procedia Comput. Sci.*, vol. 132, pp. 679–688, 2018.

[14] G. L. Shen and X. J. Wu, "Content based image retrieval by combining color, texture and CENTRIST," in *Proc. Constantinides Int. Workshop Signal Process.*, 2013, pp. 1–4.

[15] W. Chen, A. Mouche, P. Tandeo, J. Stopa, and D. Vandemark, "Automated geophysical classification of Sentinel-1 wave mode SAR images through deep-learning," in *Proc. IEEE Int. Geosci. Remote Sens. Symp.*, 2018, pp. 1776–1779.

[16] W. Shao, Y. Sheng, and S. Jian, "Preliminary assessment of wind and wave retrieval from Chinese Gaofen-3 SAR imagery," *Sensors*, vol. 17, no. 8, 2017, Art. no. 1705.

[17] W. Shao *et al.*, "Evaluation of wind retrieval from co-polarization Gaofen-3 SAR imagery around China Seas," *J. Ocean Univ. China*, vol. 18, no. 2, pp. 1–13, 2019.

[18] J. Sun, W. D. Yu, and Y. K. Deng, "The SAR payload design and performance for the GF-3 mission," *Sensors*, vol. 17, no. 10, Oct. 2017, Art. no. 2419, doi: 10.3390/s17102419.

[19] C. Wang, A. Mouche, P. Tandeo, J. E. Stopa, and B. Chapron, "A labelled ocean SAR imagery dataset of ten geophysical phenomena from Sentinel-1 wave mode," *Geosci. Data J.*, vol. 6, pp. 105–115, 2019.

[20] B. W. Atkinson and J. W. Zhang, "Mesoscale shallow convection in the atmosphere," *Rev. Geophys.*, vol. 34, no. 4, pp. 403–431, 1996.

[21] C. Jackson, *Synthetic Aperture Radar Marine User's Manual*. Washington, DC, USA: U.S. Dept. Commerce, 2004.

[22] G. S. Young, D. Kristovich, M. R. Hjelmfelt, and R. C. Foster, "Rolls, streets, waves, and more: A review of quasi-two-dimensional structures in the atmospheric boundary layer," *Bull. Amer. Meteorol. Soc.*, vol. 83, no. 7, pp. 1001–1001, 2002.

[23] Y. X. Cheng, A. I. Wei-Hua, Y. Kong, and X. B. Zhao, *Ocean Wind Retrieval From Spaceborne Synthetic Aperture Radar Images Based on Wind Streaks and External Wind Direction*. Ledyard, CT, USA: Mar. Sci., 2015.

[24] W. Alpers, "ERS-1 SAR views the ocean: An assessment," in *Proc. Int. Geosci. Remote Sens. Symp.*, 1994, vol. 4, pp. 1951–1953.

[25] M. Z. Alom, T. M. Taha, C. Yakopcic, S. Westberg, and V. K. Asari, "The history began from AlexNet: A comprehensive survey on deep learning approaches," 2018, *arXiv:1803.01164*.

[26] C. Szegedy, V. Vanhoucke, S. Ioffe, J. Shlens, and Z. Wojna, "Rethinking the inception architecture for computer vision," in *Proc. IEEE Conf. Comput. Vis. Pattern Recognit.*, 2016, pp. 2818–2826.

[27] O. M. Albatayneh, L. Forslöf, and K. Ksaibati, "Image retraining using tensorflow implementation of the pre-trained Inception-V3 model for evaluating gravel road dust," *J. Infrastruct. Syst.*, vol. 26, no. 2, pp. 268–276, 2020.

[28] A. Elyouncha, L. Eriksson, R. Romeiser, and L. Ulander, "Wind direction ambiguity removal using along-track Insar: A case study," in *Proc. IEEE Int. Geosci. Remote Sens. Symp.*, 2018, pp. 3262–3265.

[29] L. Zhou, G. Zheng, X. Li, J. Yang, and X. Lou, "An improved local gradient method for sea surface wind direction retrieval from SAR imagery," *Remote Sens.*, vol. 9, no. 7, 2017, Art. no. 671.

[30] Y. Kong, X. B. Zhao, W. H. Ai, D. Han, and J. Xue, "Ocean surface wind field retrieval from airborne SAR imagery based on Mexican-hat wavelet transform," *Jiefangjun Ligong Daxue Xuebao/J. PLA Univ. Sci. Technol.*, vol. 12, no. 3, pp. 301–306, 2011.

[31] N. Melia, K. Haines, and E. Hawkins, "Sea ice decline and 21st century trans-Arctic shipping routes," *Geophys. Res. Lett.*, vol. 43, no. 18, pp. 9720–9728, Sep. 2016.

[32] J. Qiao, W. Ai, X. Hu, S. Hu, and X. Du, "Characteristics of melting layer in cyclones over the western North Pacific detected by the GPM dual-frequency precipitation radar," *Earth Space Sci.*, vol. 9, no. 3, Mar. 2012, Art. no. e2021EA001967.

[33] W. A. J. Qiao, X. Hu, M. Liu, and S. Hu, "An identification method of melting layer using the covariance wavelet transform based on GPM-DPR observations," *Earth Space Sci.*, vol. 9, no. 3, Mar. 2012, Art. no. e2021EA002103.

Chaogang Guo received the B.S. degree in atmospheric science from the National University of Defense Technology, Nanjing, China, in 2020, where he is currently working toward the M.S. degree in atmosphere science.

His research interests include atmospheric physics, radar, and remote sensing techniques and instruments.
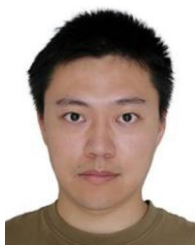
Weihua Ai received the B.S., M.S., and Ph.D. degrees in atmosphere science from the PLA University of Science and Technology, Nanjing, China, in 2002, 2004, and 2007, respectively.

He is currently an Associate Professor with the College of Atmosphere and Sea, National University of Defense Technology, Nanjing, China. His research interests include radar simulator and microwave remote sensing.

Xiaoyong Du received the B.S. and M.S. degrees in atmospheric physics and atmospheric environment from the University of Chinese Academy of Science, Hefei, China, in 2004 and 2007, respectively.

He is currently an Engineer with the National University of Defense Technology, Nanjing, China. His research interests include meteorological and marine environmental monitoring technology.

Shensen Hu received the B.S. degree in radar engineering from the PLA University of Science and Technology, Nanjing, China, in 2014, and the Ph.D. degree in atmospheric science from the National University of Defense Technology, Changsha, China, in 2019.

He is currently a Lecturer with the National University of Defense Technology. His research interests include radar meteorology and low-light satellite remote sensing.
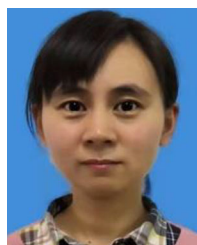
Nan Chen received the B.S. degree in atmospheric remote sensing science and technology from the Nanjing University of Information Science and Technology, Nanjing, China, in 2008.

She is currently an Associate Professor with the College of Meteorology and Oceanography, National University of Defense Technology, Nanjing, China. She has been engaged in the teaching and scientific research of radar meteorology for decades.